

2012

## Crystal structure, electronic structure and thermoelectric properties of n-type BiSbSTe<sub>2</sub>

Sima Aminorroaya-Yamini  
*University of Wollongong*, [sima@uow.edu.au](mailto:sima@uow.edu.au)

Chao Zhang  
*University of Wollongong*, [czhang@uow.edu.au](mailto:czhang@uow.edu.au)

Xiaolin Wang  
*University of Wollongong*, [xiaolin@uow.edu.au](mailto:xiaolin@uow.edu.au)

Ivan Nevirkovets  
*University Of Wollongong*, [ivann@uow.edu.au](mailto:ivann@uow.edu.au)

Follow this and additional works at: <https://ro.uow.edu.au/engpapers>



Part of the [Engineering Commons](#)

<https://ro.uow.edu.au/engpapers/5064>

---

### Recommended Citation

Aminorroaya-Yamini, Sima; Zhang, Chao; Wang, Xiaolin; and Nevirkovets, Ivan: Crystal structure, electronic structure and thermoelectric properties of n-type BiSbSTe<sub>2</sub> 2012, 1-6.  
<https://ro.uow.edu.au/engpapers/5064>

# Crystal structure, electronic structure and thermoelectric properties of *n*-type BiSbSTe<sub>2</sub>

Sima Aminorroaya-Yamini,\* Chao Zhang, Xiaolin Wang and Ivan Nevirkovets

Institute for Superconducting and Electronic Materials (ISEM), University of Wollongong, North Wollongong, NSW 2519, Australia, Email: sima@uow.edu.au

**Abstract.** *N*-type bismuth telluride sulphide has received attention as a potential thermoelectric material due to its large thermopower and ability to form solid solutions with bismuth antimony sulphide. Here, we fabricated an *n*-type tetradymite BiSbSTe<sub>2</sub> by solid state reaction. The crystal structure was found to be rhombohedral, and the thermoelectric properties were measured for the temperature range of 50-390 K. A high Seebeck coefficient of -190 μV/K was achieved at 385 K. The electronic structure of BiSbSTe<sub>2</sub> was investigated by using first-principles calculations and compared with its parent counterpart (Bi<sub>2</sub>STe<sub>2</sub>). The results have shown that BiSbSTe<sub>2</sub> is a narrow band gap semiconductor. For the first time, we have demonstrated that the vacancies in substitutional atomic sites, which can be altered through different fabrication techniques, can determine the charge carrier nature of tetradymite thermoelectrics. As a proof of concept, we have shown that the vacancies in antimony sites result in a *p*-type compound while a sulphur deficiency produces an *n*-type phase with lower electrical conductivity.

## Introduction

Reversible thermoelectric heat to electric energy convertors will likely play a significant role in clean and renewable energy, and reduce the reliance on fossil-fuelled heat engines that generate approximately 90% of the world's power at typical 30-40% efficiency [1]. Although thermoelectric modules have been used for quite some time in niche applications, the low thermoelectric effect and high price of thermoelectric materials have limited their widespread application [2]. The efficiency of thermoelectric materials is defined by the dimensionless figure of merit,  $ZT = S^2 T \sigma / \kappa$ , or the power factor,  $P = S^2 \sigma$ , which are functions of thermal conductivity ( $\kappa$ ), Seebeck coefficient ( $S$ ), electrical conductivity ( $\sigma$ ), and absolute temperature. The figure of merit increases with thermoelectric efficiency and is achieved by either enhancement of the power factor and/or by decreasing the thermal conductivity through alloying and/or nanostructuring [3]. It is elegantly shown that nanostructured thermoelectric materials exhibit higher  $ZT$  compared to their bulk counterparts, due to a reduction in thermal conductivity by energy scattering mechanisms and/or an increase in thermopower ( $S$ ) from quantum effects [4-6]. However, thin-film superlattices and nanowires cannot be used for high volume applications, and nanostructuring should be utilized on bulk materials.

Tetradymite compounds present attractive properties for possible thermoelectric materials. Tetradymite type crystals are narrow band-gap semiconductors with the composition  $A_2B_3$  and represent one of the most well-known thermoelectric materials. Bismuth telluride based alloys demonstrate the highest figures of merit, and are the most commercialised thermoelectric materials over the temperature range of 200-400 K [7-9]. However, the figure of merit of *n*-type materials is much lower than for *p*-type thermoelectric materials due to difficulties in controlling the doping element concentration [10]. Therefore, there is a need to seek new *n*-type semiconductors. Recently,

bismuth telluride sulphide,  $\text{Bi}_2\text{Te}_2\text{S}$ , has received attention as a potential *n*-type thermoelectric material, due to its large Seebeck coefficient and ability to form single phase solid solutions with  $\text{Sb}_2\text{Te}_2\text{S}$  [11]. Our choice of fabrication technique was motivated by a report which suggested that figure of merit values and power factor values of thermoelectric materials might be influenced by fabrication techniques that affect the thermal conductivity and carrier concentration [4, 12]. Understanding the origins of this influence is important for development of new thermoelectric materials. In the work conducted here,  $\text{Bi}_{0.5}\text{Sb}_{1.5}\text{Te}_3$  and  $\text{Bi}_2\text{S}_3$  powders were employed as raw materials to fabricate single phase  $\text{BiSbSTe}_2$ , while previous studies synthesized the compound either through the reaction of the elements Bi, Sb, Te, and S [11, 13] or by chemical synthesis [14, 15]. The thermoelectric properties and crystal structure of the single phase materials are studied and compared with previous reports. To the best of the authors' knowledge, no theoretical investigation has been reported for this compound.

In the present study, we have also theoretically examined the electronic structure of  $\text{BiSbSTe}_2$  by using first principles band structure calculations.

## Experimental

*P*-type  $\text{Bi}_{0.5}\text{Sb}_{1.5}\text{Te}_3$  compound and pure  $\text{Bi}_2\text{S}_3$  powder from Sigma Aldrich were used to synthesise the single phase  $\text{BiSbSTe}_2$  alloy. Stoichiometric quantities of  $\text{Bi}_{0.5}\text{Sb}_{1.5}\text{Te}_3$  and  $\text{Bi}_2\text{S}_3$  powders were mixed with an agate mortar and pestle, and uniaxially pressed at 40 MPa to produce a 10 mm diameter pellet. The pellets were loaded into cleaned and dried quartz tubes, sealed under vacuum, premelted at 600°C for 12 hours, quenched in water, and then annealed at 500°C for approximately three days, until a single phase material was obtained. A PANalytical, X'Pert Pro MRD X-ray diffractometer (XRD) with Cu  $K\alpha$  radiation ( $\lambda = 1.544 \text{ \AA}$ , 40 kV, 30 mA) was used for phase analysis and structural characterisation of the sample. The XRD patterns were analysed by Rietveld refinement, using the Rietica software package. The chemical composition of the phase was confirmed by X-ray photoelectron spectroscopy (XPS), performed on a XPS PHOIBOS 100 hemispherical analyser (SPECS GmbH) using monochromatic Al  $K\alpha$  X-rays as the exciting source. Temperature dependent thermal and electronic transport properties were measured in a Quantum Design Physical Properties Measurement System (PPMS), using the standard four probe method. It is worth noting that different ratios of primary compounds ( $\text{Bi}_{0.5}\text{Sb}_{1.5}\text{Te}_3$  and  $\text{Bi}_2\text{S}_3$ ) were alloyed to introduce various amount of sulphur to the final fabricated phase. However, the results to be reported elsewhere indicate the coexistence of two phases on those samples.

## Results and discussion

In order to study the crystal structure of the compound, the X-ray diffraction pattern of  $\text{BiSbSTe}_2$  was indexed and refined using Rietveld analysis and employment of the rhombohedral model [16]. Figure 1 presents an XRD pattern of the single crystallized phase. A schematic of the crystal structure, the primary unit cell, and the atomic layers of the  $\text{BiSbSTe}_2$  are shown in Figure 2(a) to (c), respectively.  $\text{BiSbSTe}_2$  crystallizes in the rhombohedral space group  $R\bar{3}m$ . The structure is composed of plates, made up of five atomic layers (Te1 – Sb – S – Bi – Te2). The plates are stacked by van der Waals interactions along the *c*-axis in the unit cell, where Sb replaces Bi in the  $\text{Bi}_2\text{STe}_2$  parent compound.

The lattice parameters of  $\text{BiSbSTe}_2$  ( $a = 4.188 \text{ \AA}$  and  $c = 29.519 \text{ \AA}$ ) are smaller than those of  $\text{Bi}_2\text{STe}_2$  ( $a = 4.238 \text{ \AA}$  and  $c = 29.589 \text{ \AA}$ ) [16] and clearly demonstrate that the unit cell volume is decreased. This is due to the substitution of antimony for bismuth, as Sb has a smaller atomic radius in the rhombohedral structure of  $\text{Bi}_2\text{Te}_2\text{S}$ . Highly symmetric semiconductor crystals tend to produce high band degeneracy [3]. The band degeneracy is defined as multiple locations in the semiconductor electron orbitals with equivalent energy. With regards to Boltzmann transport theory, larger band degeneracy enhances the effective mobility of electrons and consequently greatly enhances thermopower [2]. Therefore we anticipate that the  $\text{BiSbSTe}_2$  phase will show a high thermopower. Thermal conductivity ( $\kappa$ ), electrical resistivity ( $\rho$ ), Seebeck coefficient ( $S$ ), and figure of merit ( $ZT$ ) values of  $\text{BiSbSTe}_2$  compound are presented in Figure 3 for the temperature range of 50-390 K. A high thermopower value of  $-190 \mu\text{V/K}$  was obtained at 385 K as expected.

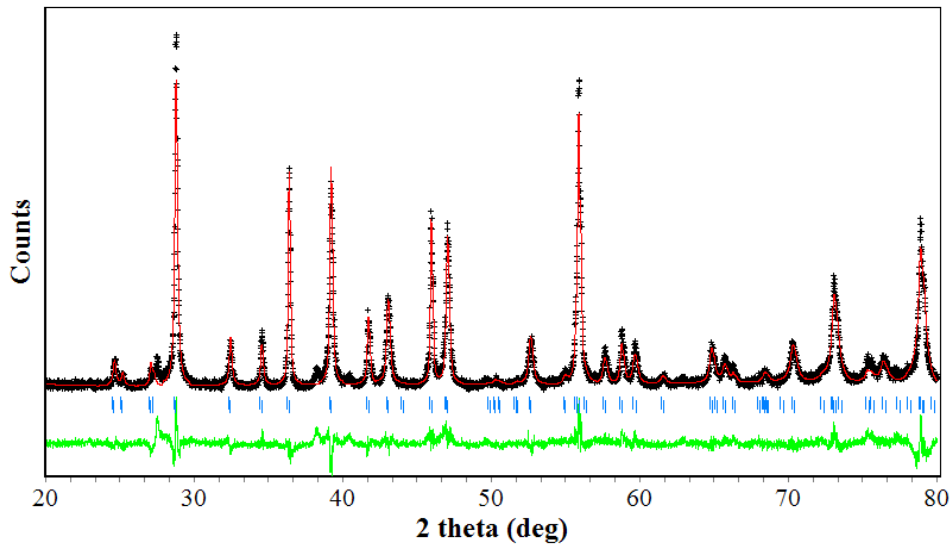


**Figure 1:** Room temperature powder X-ray diffraction pattern (symbols) for  $\text{BiSbSTe}_2$  from  $20^\circ$  to  $80^\circ$ , together with standard peak positions (blue vertical lines) and fit (solid line) of the model to intensities. The green solid line at the bottom is the difference spectrum.

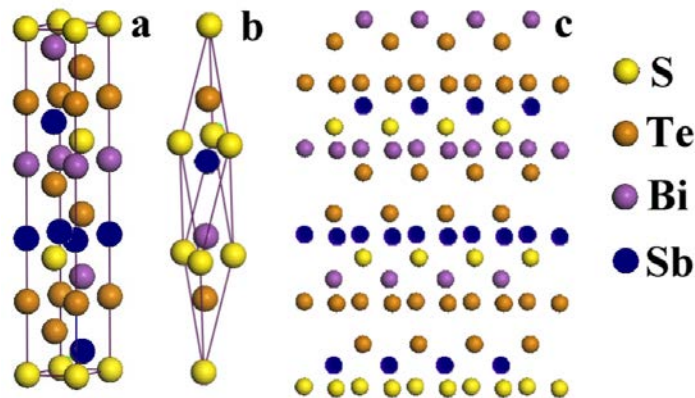


**Figure 2:** (a) Schematic crystal structure of rhombohedral  $\text{BiSbSTe}_2$ , (b) the primary unit cell, and (c) five atomic layers stacked along the  $c$ -axis by van der Waals interactions.

Figure 3(a) shows that thermal conductivity increases and electrical resistivity decreases with increasing temperature, which is typical semiconducting behaviour of thermoelectric materials [17]. The thermoelectric properties of BiSbSTe<sub>2</sub> compound studied here at room temperature have been compared with the results for BiSbSTe<sub>2</sub> and Bi<sub>2</sub>STe<sub>2</sub> extracted from the literature [11] in Table 1.

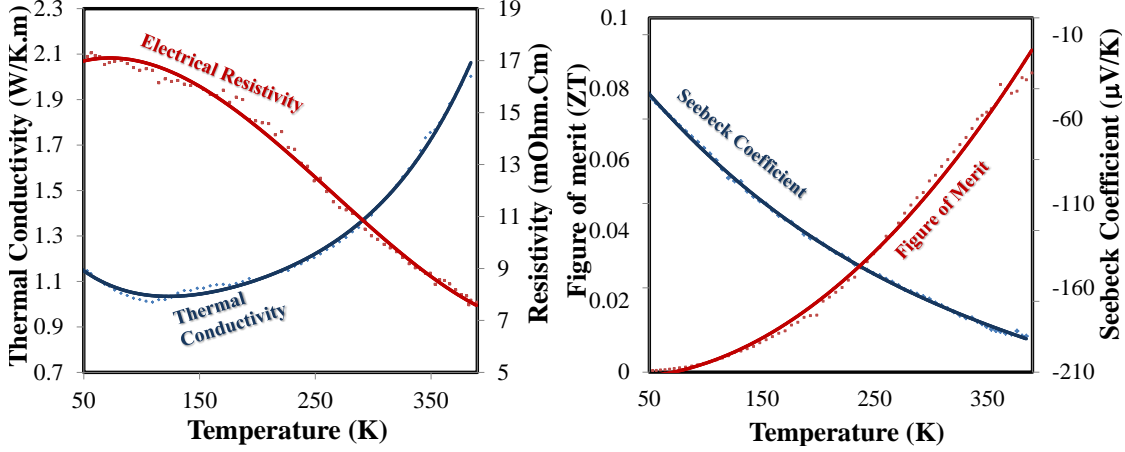


**Figure 3: Thermal conductivity ( $\kappa$ ) and resistivity ( $\rho$ ), Seebeck coefficient ( $S$ ) and figure of merit ( $ZT$ ) of BiSbSTe<sub>2</sub> compound over the 50 to 390 K temperature range**

**Table 1: Room temperature Seebeck coefficient ( $S$ ), electrical conductivity ( $\sigma$ ), and thermal conductivity ( $\kappa$ ) of BiSbSTe<sub>2</sub> and Bi<sub>2</sub>STe<sub>2</sub>**

	$S$ ( $\mu\text{V/K}$ )	$\sigma$ (mohm·cm)	$\kappa$ (W/Km)
<b>BiSbSTe<sub>2</sub></b>	-170	9.9	1.429
<b>BiSbSTe<sub>2</sub> [11]</b>	150	1.9	1.4
<b>Bi<sub>2</sub>STe<sub>2</sub> [11]</b>	-170	2.5	1.6

The Seebeck coefficient value of our sample demonstrates that it is an *n*-type thermoelectric compound, while a previous study [11] shows a *p*-type thermoelectric material, with the absolute value of the Seebeck coefficient (120  $\mu\text{V/K}$ ) less than in the current study (-170  $\mu\text{V/K}$ ). This disparity may be attributed to differences in lattice defects due to the various fabrication techniques. In the present study, bismuth sulphide (Bi<sub>2</sub>S<sub>3</sub>) and *p*-type Bi<sub>0.5</sub>Sb<sub>1.5</sub>Te<sub>3</sub> were chosen to make single phase BiSbSTe<sub>2</sub>, while the phase was synthesized from the individual elements by Grauer et al.[11], with up to 10% Sb<sub>2</sub>Te<sub>3</sub> phase reported as an impurity in their final compound. Moreover, different fabrication techniques may introduce various crystal defects and/or atomic vacancies into the crystal lattice. Several attempts [18-21] have been made to study the effect of point defects on charge carrier type in bismuth telluride through various fabrication techniques. It is shown that vacancies and antisite defects, i.e. replacement of Te atoms on a Te sublattice by Bi atoms or replacement of Bi atoms on a Bi sublattice by Te atoms, play the significant role on charge carrier nature. Whereas, chemical environment and growth conditions lead to different defects and consequently various charge carrier type and thermopower [22]

In order to study the effects of elemental deficiencies on the electronic states of the alloy (BiSbSTe<sub>2</sub>), we performed first-principles band structure calculations using density functional theory [23] and compared the results with the parent Bi<sub>2</sub>STe<sub>2</sub> compound. It is pertinent to note that the calculations were performed on two hypothetical BiSbS<sub>0.5</sub>Te<sub>2</sub> and BiSb<sub>0.5</sub>STe<sub>2</sub> phases in order to evaluate the effects of sulphur and antimony deficiency, respectively, on the electronic properties of the compound. This assessment will be made when the electronic structure of BiSbSTe<sub>2</sub> has been discussed in the following section.

We adopted the standard generalized gradient approximation, with the Perdew-Burke-Ernzerhof functional. Lattice parameters and atomic positions obtained from the Rietveld refinement for the BiSbSTe<sub>2</sub> were used as structural parameters for the calculations. A bismuth atom replaces one antimony atom, and one sulphur atom replaces a tellurium atom in the unit cell (shown in Figure 2). This makes the atomic ratio Bi:Sb:S:Te = 1:1:1:2. A 4×4×4 k mesh was used for Brillouin sampling, with cut-off energy of 220 eV to allow ultra-fast calculation of pseudo-potentials for band structure calculations, while a 7×7×7 k mesh was chosen as the Monkhorst-Pack grid for density of states calculations.

Figure 4 shows the calculated band structure of Bi<sub>2</sub>STe<sub>2</sub> and BiSbSTe<sub>2</sub>. Both compounds are narrow band gap semiconductors with direct gaps of approximately 0.29 eV and 0.2 eV respectively. The conduction band minimum and valence band maximum at the  $\Gamma$ -point represent a direct band gap of 0.2 eV in the BiSbSTe<sub>2</sub> compound. Around the  $\Gamma$ -point, the charge carrier effective mass (electron or hole),  $m^*$ , can be defined by equation (1), where,  $\hbar$  is the Dirac constant and  $k$  is the wave vector.

$$\frac{1}{m^*} = \left(\frac{1}{\hbar^2}\right) \left(\frac{\partial^2 E}{\partial k^2}\right) \quad (1)$$

The charge carrier effective mass of BiSbSTe<sub>2</sub> in both valence and conduction bands is heavier than in Bi<sub>2</sub>STe<sub>2</sub> compound. It appears that replacement of Bi with Sb results in a narrower band gap and heavier bands.

The calculated partial densities of states of each atom for BiSbSTe<sub>2</sub> are shown in Figure 5 within the -14 eV to 10 eV energy range. The density of states (DOS) between -14 eV and 7 eV is formed by s states, while the (DOS) within -4 eV to the zero energy range is mainly contributed from p states. Moreover, the (DOS) of the valence band near Fermi level is dominated by Bi-s, Sb-s and Te-p and S-p states. However, it is only the Te-s states and p states of Sb, S and Bi that form the (DOS) of the conduction bands near the Fermi level ( $E_F$ ). Figure 5 shows that the Sb-s and Bi-s states are mainly concentrated at higher binding energy and hybridize with the Te-s and S-p states, whereas in the upper valence band, the hybridizing between Sb-s and S-p, and Bi-s and Te-p are the strongest, so that the bond distances between Sb-S and Bi-Te are shorter than the other bond distances, as is experimentally confirmed in Table II, where the bond distances are demonstrated from Rietveld refinement.

**Table 2: The bond distances in BiSbSTe<sub>2</sub> compound attained from Rietveld refinement**

<b>Atom1</b>	Bi	Bi	Bi	Bi	Sb	Sb	Sb	S	Te
<b>Atom2</b>	Bi	Sb	S	Te	Sb	S	Te	Te	Te
<b>Distance (Å)</b>	4.188	4.224	3.302	2.716	4.177	2.958	3.004	4.242	3.754

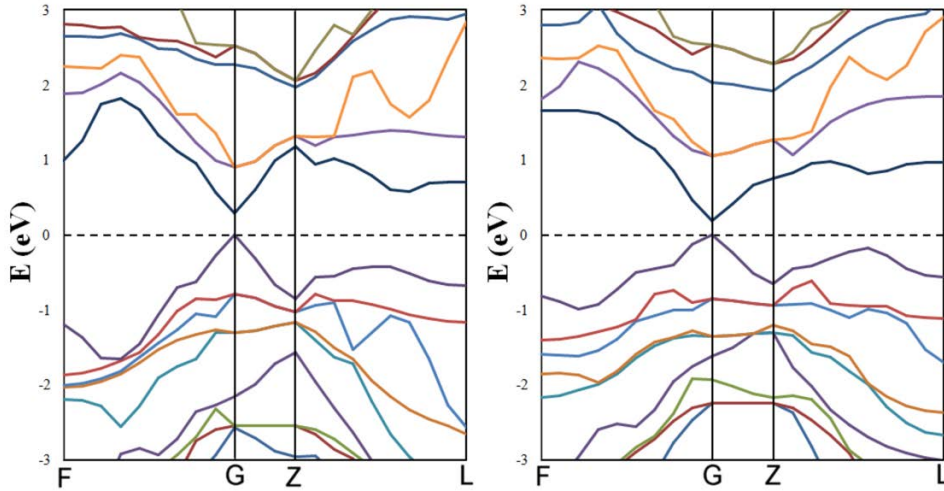


**Figure 4: Electronic band structure of  $\text{Bi}_2\text{STe}_2$ (left) and  $\text{BiSbSTe}_2$ (right). Top of the valence band is set to zero.**

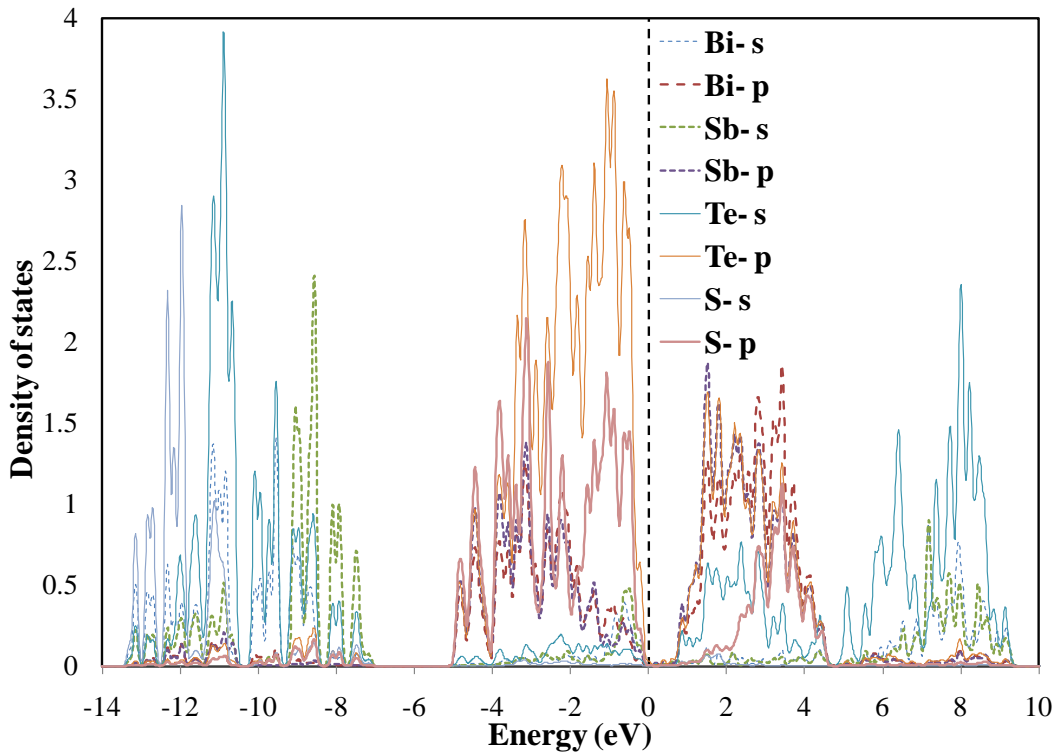


**Figure 5: Calculated partial density of states of  $\text{BiSbSTe}_2$ , within the energy range of -15 eV to 10 eV for Bi, Sb, S and Te. Top of the valence band is set to zero**

For a more in depth study of the effects of sulphur and antimony deficiency on the electronic states of  $\text{BiSbSTe}_2$ , the total density of states (DOS) for  $\text{BiSbSTe}_2$  phase together with hypothetical  $\text{BiSbS}_{0.5}\text{Te}_2$  and  $\text{BiSb}_{0.5}\text{STe}_2$  compounds are presented in Figure 6. It is clearly shown that the Fermi level penetrates into the conduction band with electrons as charge carriers when there is a sulphur deficiency (Figure 6(b)), while antimony deficiency (Figure 6(c)) moves the Fermi level energy to the valence band with holes as charge carriers, which results in *p*-type thermoelectric behaviour. This result indicates that the atomic vacancies play a crucial role with respect to the nature of the charge carrier. It can also be concluded that the technique which was chosen to fabricate  $\text{BiSbSTe}_2$  in the present study may result in sulphur deficiency, while the phase fabricated by Grauer et al. [11] has

antimony deficiency. They have reported the formation of impurity  $\text{Sb}_2\text{Te}_3$  phase in their final compound and therefore it is anticipated that antimony has been removed from the final  $\text{BiSbSTe}_2$  phase and lead to antimony deficiency. However, in the current study, liquid  $\text{BiSbS}_{0.5}\text{Te}_2$  is reacted with solid  $\text{Bi}_2\text{S}_3$  at premelting temperature. It is worth noting that due to volatility of sulphur, bismuth sulphide has intrinsic sulphur deficiency [24]. Hence, it is expected that final compound of the present study has sulphur deficiency attributed to the starting raw materials. In order to confirm this hypothesis, X-ray photoelectron spectroscopy (XPS) was employed to evaluate the composition and purity of the phase. XRD results (Figure 1) confirmed that the compound is a single phase, and therefore the composition of the sample surface can be an adequate representative of the bulk composition.

A typical wide-scan XPS spectrum of the phase is shown in Figure 7(a), in which all peaks can be assigned to the elements Bi, Sb, S, and Te. Two strong peaks at 528.8 and 538.2 eV in the high resolution XPS spectra (Figure 7(b)) are assigned to  $\text{Sb}(3d_{5/2})$  and  $\text{Sb}(3d_{3/2})$ , respectively. The peak at 225.8 eV confirms the S (2s) transition, and peaks at 572 and 582.2 eV in Figure 7(c) correspond to  $\text{Te}(3d_{5/2})$  and  $\text{Te}(3d_{3/2})$ , respectively. The peak at 157.45 eV is assigned to  $\text{Bi}(4f_{5/2})$ , and the peak at 162.8 eV is a composite of  $\text{Bi}(4f_{7/2})$  and  $\text{S}(2p_{3/2})$ , as shown in the Figure 7(d) inset. The elemental composition of the compound in the Figure 7(d) inset shows the sulphur deficiency in the final compound, which evidently supports the band structure calculation. Therefore, we demonstrate that sulphur deficiency in  $\text{BiSbSTe}_2$  results in *n*-type semiconductor behaviour.

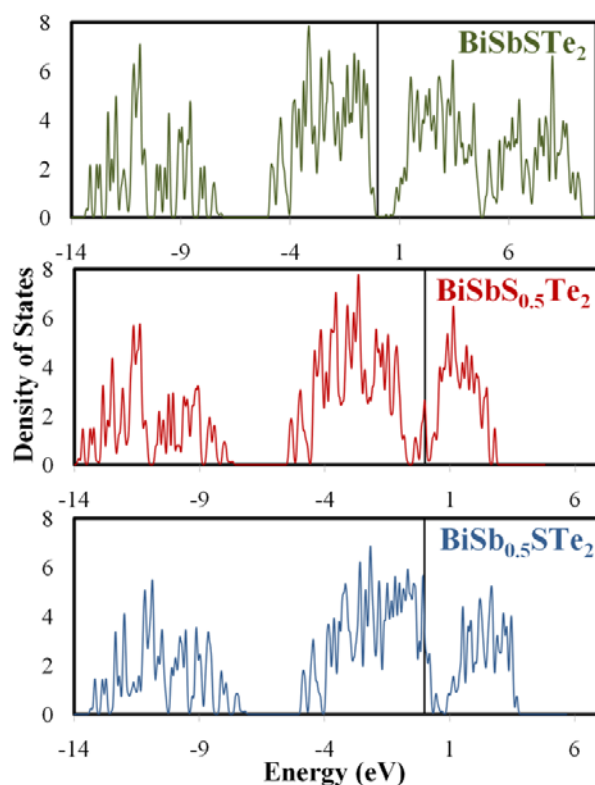


**Figure 6: Total density of states (DOS) of atoms for  $\text{BiSbSTe}_2$  phases and for hypothetical  $\text{BiSbS}_{0.5}\text{Te}_2$  and  $\text{BiSb}_{0.5}\text{STe}_2$  compounds calculated by first principles band structure calculations**



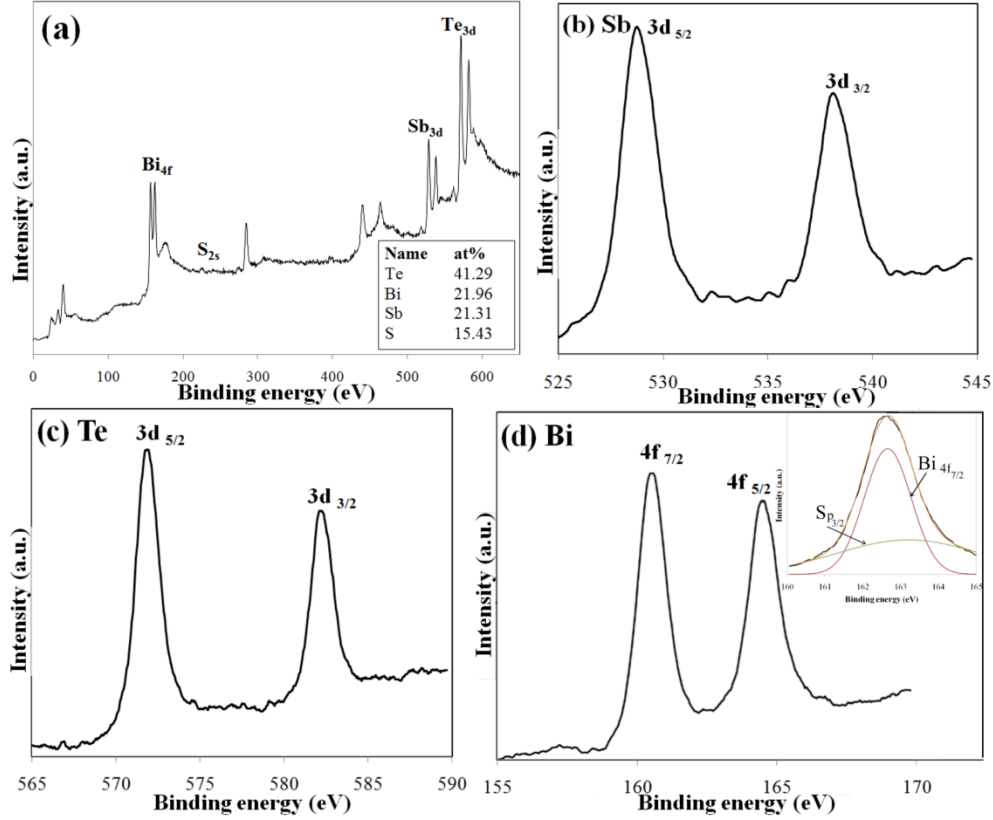


**Figure 7: XPS spectra of BiSbSTe<sub>2</sub>: (a) general scan; high resolution scans of (b) the antimony region (Sb3d), (c) the tellurium region (Te3d), and (d) the bismuth region (4f), with the inset giving a detailed fit of one of the peaks.**

It remains to determine the specific influence of the band structure on the electrical conductivity. The electrical conductivity in semiconductors is obtained from equation (2) based on Boltzmann transport theory, where  $q=-e$  for electrons and  $+e$  for holes,  $f$  is the distribution function of charge carriers,  $\tau$  is relaxation time and  $D(E)$  is the density of states

$$\sigma = -\frac{2q^2}{3m} \int_{E=0}^{\infty} \frac{\partial f_0}{\partial E} D(E) E \tau dE \quad (2)$$

For a given Fermi level, an increase in DOS will lead to a higher electrical conductivity. Furthermore, Figure 6(b) and (c) shows that  $D(\epsilon)$  is higher in the case of antimony deficiency rather than sulphur deficiency, and consequently, it is expected that the  $p$ -type compound (BiSbSTe<sub>2</sub> phase with Sb deficiency) would show higher electrical conductivity due to higher charge carrier concentration than the phase with sulphur deficiency ( $n$ -type compound), which is consistent with the results shown in Table II, where electrical conductivity of  $p$ -type BiSbSTe<sub>2</sub> compound [11] is considerably higher than for  $n$ -type BiSbSTe<sub>2</sub> phase (current study).

## Conclusions

We have successfully fabricated tetradymite  $n$ -type BiSbSTe<sub>2</sub> with a high Seebeck coefficient of  $-190 \mu\text{V/K}$  at 385 K and reported the transport properties of the BiSbSTe<sub>2</sub> compound for the temperature range of 50 to 390 K. Our first principles calculations of electronic structures support experimental findings in terms of bond energy and thermoelectric behaviour. Thermoelectric properties measurements and first-principles calculations have demonstrated that different fabrication techniques

lead to various crystal defects and atomic vacancies which result in *n*-type or *p*-type semiconductors. Therefore, it is possible in principle to alter the semiconducting type (charge carrier nature) by introducing vacancies on substituted atoms. The approaches used in the present study may also be useful as a guideline for future development of thermoelectric materials and study of the potential applications of tetradymite-type BiSbSTe<sub>2</sub> in thermoelectrics.

### Acknowledgement

This work was supported by an International Science Linkage grant funded by the Department of Industry, Innovation, Science and Research.

### References

1. Hochbaum, A.I., R. Chen, R.D. Delgado, W. Liang, E.C. Garnett, M. Najarian, A. Majumdar, and P. Yang, *Enhanced thermoelectric performance of rough silicon nanowires*. Nature, 2008. **451**(7175): p. 163-167.
2. Pei, Y., X. Shi, A. LaLonde, H. Wang, L. Chen, and G.J. Snyder, *Convergence of electronic bands for high performance bulk thermoelectrics*. Nature, 2011. **473**(7345): p. 66-69.
3. Sootsman, J.R., D.Y. Chung, and M.G. Kanatzidis, *New and Old Concepts in Thermoelectric Materials*. Angewandte Chemie International Edition, 2009. **48**(46): p. 8616-8639.
4. Zhao, Y., J.S. Dyck, B.M. Hernandez, and C. Burda, *Enhancing thermoelectric performance of ternary nanocrystals through adjusting carrier concentration*. Journal of American Chemical Society, 2010. **132**(14): p. 4982-4983.
5. Wang, T., R. Mehta, C. Karthik, P.G. Ganesan, B. Singh, W. Jiang, N. Ravishankar, T. Borca-Tasciuc, and G. Ramanath, *Microsphere bouquets of bismuth telluride nanoplates: Room-temperature synthesis and thermoelectric properties*. Journal of Physical Chemistry C, 2010. **114**: p. 1796-1799.
6. Pernot, G., M. Stoffel, I. Savic, F. Pezzoli, P. Chen, G. Savelli, A. Jacquot, J. Schumann, U. Denker, I. Mönch, C. Deneke, O.G. Schmidt, J.M. Rampnoux, S. Wang, M. Plissonnier, A. Rastelli, S. Dilhaire, and N. Mingo, *Precise control of thermal conductivity at the nanoscale through individual phonon-scattering barriers*. Nat Mater, 2010. **9**(6): p. 491-495.
7. Yamashita, O., S. Tomiyoshi, and K. Makita, *Bismuth telluride compounds with high thermoelectric figures of merit*. Journal of Applied Physics, 2003. **93**(1): p. 368-374.
8. Snyder, G.J. and E.S. Toberer, *Complex thermoelectric materials*. Nature Materials, 2008. **7**: p. 105-114.
9. Xie, W., X. Tang, Y. Yan, Q. Zhang, and T.M. Tritt, *Unique nanostructures and enhanced thermoelectric performance of melt-spun BiSbTe alloys*. Applied Physics Letters, 2009. **94**: p. 102111.
10. Han, M.-K., K. Ahn, H. Kim, J.-S. Rhyee, and S.-J. Kim, *Formation of Cu nanoparticles in layered Bi<sub>2</sub>Te<sub>3</sub> and their effect on ZT enhancement*. Journal of Materials Chemistry, 2011. **21**(30): p. 11365-11370.
11. Grauer, D.C., Y.S. Hor, A.J. Williams, and R.J. Cava, *Thermoelectric properties of the tetradymite-type Bi<sub>2</sub>Te<sub>2</sub>S-Sb<sub>2</sub>Te<sub>2</sub>S solid solution*. Materials Research Bulletin, 2009. **44**(9): p. 1926-1929.
12. Urban, J.J., D.V. Talapin, E.V. Shevchenko, C.R. Kagan, and C.B. B. Murray, *Synergism in binary nanocrystal superlattices leads to enhanced p-type conductivity in self-assembled PbTe/Ag<sub>2</sub>Te thin films*. Nature Materials, 2007. **6**: p. 115-121.
13. Lee, D.M., C.H. Lim, S.Y. Shin, and C.H. Lee, *Thermoelectric properties of p-type Bi<sub>0.5</sub>Sb<sub>1.5</sub>Te<sub>3</sub> compounds fabricated by spark plasma sintering*. Journal of Electroceramics, 2006. **17**: p. 879-883.
14. Zhao, Y., J.S. Dyck, B.M. Hernandez, and C. Burda, *Enhancing Thermoelectric Performance of Ternary Nanocrystals through Adjusting Carrier Concentration*. Journal of the American Chemical Society, 2010. **132**(14): p. 4982-4983.
15. Purkayastha, A., Q. Yan, M.S. Raghuvver, D.D. Gandhi, H. Li, Z.W. Liu, R.V. Ramanujan, T. Borca-Tasciuc, and G. Ramanath, *Surfactant-Directed Synthesis of Branched Bismuth Telluride/Sulfide Core/Shell Nanorods*. Advanced Materials, 2008. **20**(14): p. 2679-2683.
16. Anthony, J.W., *Handbook of mineralogy, Tetradymite*. Vol. V. 2003, Tuscon, Arizona: Mineral Data Publishing.
17. Kittel, C., *Introduction to solid state physics*. Seventh ed. ed. 1996, New York: John Wiley & Sons, Inc.
18. Cho, S., Y. Kim, A. DiVenere, G.K. Wong, J.B. Ketterson, and J.R. Meyer, *Antisite defects of Bi<sub>2</sub>Te<sub>3</sub> thin films*. Applied Physics Letters, 1999. **75**(10): p. 1401-1403.

19. da Silva, L.W., M. Kaviany, and C. Uher, *Thermoelectric performance of films in the bismuth-tellurium and antimony-tellurium systems*. Journal of Applied Physics, 2005. **97**(11): p. 114903-10.
20. Lošt'ák, P., Č. Drašar, D. Bachan, L. Beneš, and A. Krejčová, *Defects in Bi<sub>2</sub>Te<sub>3-x</sub>Se<sub>x</sub> single crystals*. Radiation Effects and Defects in Solids, 2010. **165**(3): p. 211-215.
21. Lin, S.-S. and C.-N. Liao, *Effect of ball milling and post treatment on crystal defects and transport properties of Bi<sub>2</sub>(Se,Te)<sub>3</sub> compounds*. Journal of Applied Physics, 2011. **110**(9): p. 093707-7.
22. Hashibon, A. and C. Elsässer, *First-principles density functional theory study of native point defects in Bi<sub>2</sub>Te<sub>3</sub>*. Physical Review B, 2011. **84**(14): p. 144117.
23. Segall, M.D., P.J.D. Lindan, M.J. Probert, C.J. Pickard, P.J. Hasnip, S.J. Clark, and M.C. Payne, *First-principles simulation: ideas, illustrations and the CASTEP code* Journal of Physics: Condensed Matter, 2002. **14**: p. 2717-2744.
24. Liufu, S.C., L.D. Chen, Q. Yao, and C.F. Wang, *Assembly of one-dimensional nanorods into Bi<sub>2</sub>S<sub>3</sub> films with enhanced thermoelectric transport properties*. Applied Physics Letters, 2007. **90**(11): p. 112106.